Proceedings of 20th International Congress on Acoustics, ICA 2010

23-27 August 2010, Sydney, Australia

Transmission loss calculations for dissipative mufflers with temperature gradients

Francisco D. Denia, Antoine Antebas, José Martínez-Casas and F. Javier Fuenmayor

Centro de Investigación de Tecnología de Vehículos, Departamento de Ingeniería Mecánica y de Materiales, Universidad Politécnica de Valencia, Camino de Vera s/n, 46022 Valencia, Spain (http://www.upv.es; fdenia@mcm.upv.es)

PACS: 43.20.Mv, 43.50.Gf, 43.20.Bi

ABSTRACT

The influence of temperature and the associated gradient on the acoustic attenuation performance of automotive dissipative mufflers is studied in detail by a multidimensional analytical approach based on the mode matching method. To account for the variation of temperature within the absorbent material, a segmentation procedure is considered with a number of dissipative regions with different but axially uniform temperature. The technique is applied to dissipative reversing chamber mufflers, including the presence of an absorbent material. For validation purposes, the analytical predictions are compared with numerical calculations based on the finite element method, showing a good agreement. While the temperature does not modify the transmission loss of reactive mufflers if the ratio of the frequency to the speed of sound is considered as the abscissa, an influence is found for dissipative configurations, at least with the models of impedance and wavenumber currently available in the literature for absorbent materials. In addition, the effect of temperature gradients on the transmission loss of some selected configurations is studied.

INTRODUCTION

The presence of non-homogeneous properties in ducts and mufflers is known to modify their acoustic attenuation performance. These spatial variations can arise, for example, from uneven filling processes in dissipative mufflers [1,2], non-uniform mean flow fields [3] and temperature gradients [4]. In the latter case, several works can be found, where the influence of temperature and the associated gradients has been modelled and analysed in reactive mufflers [5,6]. It appears, however, that temperature effects for dissipative mufflers containing an absorbent material remains to be investigated. The objective of the present work is then to analyse the sound propagation in dissipative configurations including the presence of high temperature and associated gradients. The technique considered focuses on the modelling of circular dissipative reversing chamber mufflers [7] by means of a three-dimensional closed-form analytical approach based on the mode matching method. Finite element predictions are also provided for validation purposes. The influence of a number of parameters on the acoustic attenuation performance is then analysed, including the effect of temperature and its gradient.

MATHEMATICAL APPROACH

Configuration under analysis. Acoustic fields

Figure 1 shows the geometry of a circular dissipative reversing chamber muffler. As can be seen, a temperature gradient exists. The total length L is divided into an entrance region (air) of length L_0 and N dissipative regions with associated values L_1, L_2, …, L_N and homogeneous and isotropic acoustic properties, evaluated at temperature $\tilde{T}_i = (T_i + T_{i+1})/2$, for $i = 1, 2, \ldots N$.

The sound propagation is governed by the Helmholtz equation [8]

$$\nabla^2 P + \kappa^2 P = 0 \tag{1}$$

where P is the acoustic pressure, ∇^2 the Laplacian operator and κ the wavenumber, given by

$$\kappa = \begin{cases} k_0 = \omega / c_0 & \text{ducts I, II, III} \\ \tilde{k}_i = \omega / \tilde{c}_i & \text{ducts } i = 1, 2, \ldots, N \end{cases} \tag{2}$$

k_0 being the wavenumber for the air, $\tilde{k}_i$ the wavenumber associated with the absorbent material located in region i, ω the angular frequency, and c_0 and $\tilde{c}_i$ the corresponding speeds of sound. For a circular duct, the pressure can be written as [9]

$$\begin{aligned} P(r,\varphi,z) &= P_A + P_B \\ &= \sum_{m=0}^{\infty}\sum_{n=0}^{\infty}\left(A_{mn}^{+}\, \mathrm{e}^{-\mathrm{j}k_{mn}z} + B_{mn}^{+}\, \mathrm{e}^{\mathrm{j}k_{mn}z}\right)\psi_{mn}(r)\,\mathrm{e}^{-\mathrm{j}m\varphi} \\ &+ \sum_{m=1}^{\infty}\sum_{n=0}^{\infty}\left(A_{mn}^{-}\, \mathrm{e}^{-\mathrm{j}k_{mn}z} + B_{mn}^{-}\, \mathrm{e}^{\mathrm{j}k_{mn}z}\right)\psi_{mn}(r)\,\mathrm{e}^{\mathrm{j}m\varphi} \end{aligned} \tag{3}$$

where A and B are modal amplitudes associated with the incident and reflected waves, respectively, (r, φ, z) are cylindrical coordinates and the tranversal mode $\psi_{mn}(r)$ is given by the Bessel function of the first kind and order m, J_m.

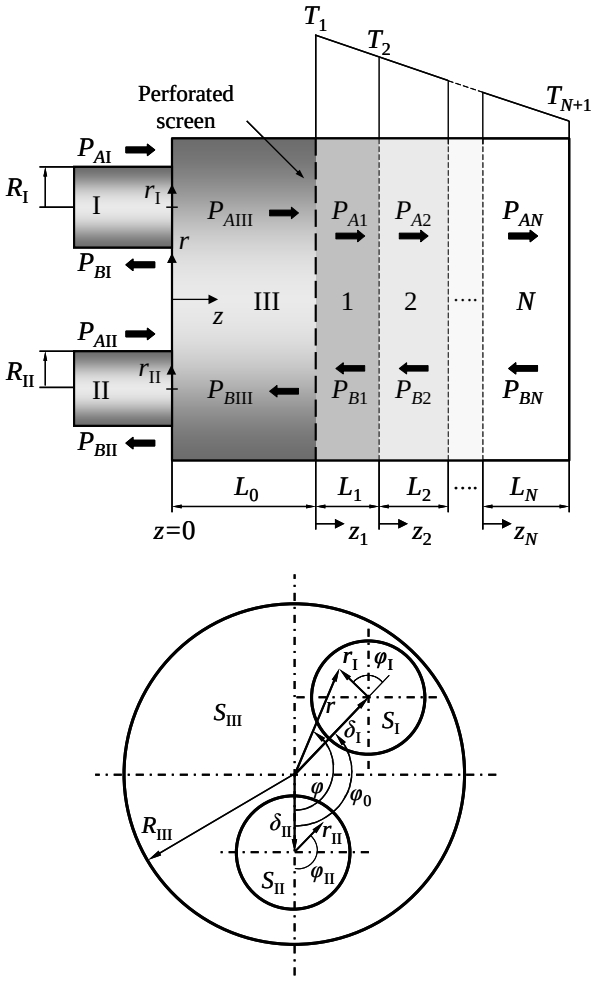

Figure 1. Geometry of a circular dissipative reversing chamber muffler with temperature gradient.

The axial wavenumber

$$k_{mn} = \pm\sqrt{\kappa^2 - \left(\alpha_{mn}/R\right)^2} \tag{4}$$

is calculated from the root α_{mn} satisfying the rigid wall boundary condition $J'_m(\alpha_{mn}) = 0$.

The axial particle velocity U is obtained from the momentum equation [9]

$$\mathrm{j}\rho\omega U = -\frac{\partial P}{\partial z} \tag{5}$$

where the density ρ is provided by

$$\rho = \begin{cases} \rho_0 & \text{ducts I, II, III} \\ \tilde{\rho}_i & \text{ducts } i = 1, 2, \ldots, N \end{cases} \tag{6}$$

The combination of Eqs. (3) and (5) yields

$$\begin{aligned} U(r,\varphi,z) &= U_A + U_B \\ &= \frac{1}{\rho\omega}\left(\sum_{m=0}^{\infty}\sum_{n=0}^{\infty} k_{mn}\left(A_{mn}^{+}\,\mathrm{e}^{-\mathrm{j}k_{mn}z} - B_{mn}^{+}\,\mathrm{e}^{\mathrm{j}k_{mn}z}\right)\psi_{mn}(r)\,\mathrm{e}^{-\mathrm{j}m\varphi} \right. \\ &\left. + \sum_{m=1}^{\infty}\sum_{n=0}^{\infty} k_{mn}\left(A_{mn}^{-}\,\mathrm{e}^{-\mathrm{j}k_{mn}z} - B_{mn}^{-}\,\mathrm{e}^{\mathrm{j}k_{mn}z}\right)\psi_{mn}(r)\,\mathrm{e}^{\mathrm{j}m\varphi} \right) \end{aligned} \tag{7}$$

Pressure and velocity conditions

These conditions can be written as follows. For the expansion and contraction, located at the left side of the muffler:

$$P_{\mathrm{I}}(r_{\mathrm{I}},\varphi_{\mathrm{I}},z=0) = P_{\mathrm{III}}(r,\varphi,z=0) \quad \text{on } S_{\mathrm{I}} \tag{8}$$

$$P_{\mathrm{II}}(r_{\mathrm{II}},\varphi_{\mathrm{II}},z=0) = P_{\mathrm{III}}(r,\varphi,z=0) \quad \text{on } S_{\mathrm{II}} \tag{9}$$

$$U_{\mathrm{I}}(r_{\mathrm{I}},\varphi_{\mathrm{I}},z=0) = U_{\mathrm{III}}(r,\varphi,z=0) \quad \text{on } S_{\mathrm{I}} \tag{10}$$

$$U_{\mathrm{II}}(r_{\mathrm{II}},\varphi_{\mathrm{II}},z=0) = U_{\mathrm{III}}(r,\varphi,z=0) \quad \text{on } S_{\mathrm{II}} \tag{11}$$

For the rigid left plate the velocity condition is

$$U_{\mathrm{III}}(r,\varphi,z=0) = 0 \quad \text{on } S_{\mathrm{III}} - S_{\mathrm{I}} - S_{\mathrm{II}} \tag{12}$$

The pressure and velocity conditions at the perforated plate can be expressed as

$$U_{\mathrm{III}}(r,\varphi,z=L_0) = U_1(r,\varphi,z_1=0) \quad \text{on } S_{\mathrm{III}} \tag{13}$$

$$\begin{aligned} &U_{\mathrm{III}}(r,\varphi,z=L_0) \\ &= \frac{P_{\mathrm{III}}(r,\varphi,z=L_0) - P_1(r,\varphi,z_1=0)}{\tilde{Z}_p} \quad \text{on } S_{\mathrm{III}} \end{aligned} \tag{14}$$

At the interface between dissipative regions i and $i + 1$, continuity of acoustic pressure and axial velocity is given by

$$P_i(r,\varphi,z_i=L_i) = P_{i+1}(r,\varphi,z_{i+1}=0) \quad \text{on } S_{\mathrm{III}} \tag{15}$$

$$U_i(r,\varphi,z_i=L_i) = U_{i+1}(r,\varphi,z_{i+1}=0) \quad \text{on } S_{\mathrm{III}} \tag{16}$$

for $i = 1, 2, \ldots, N - 1$.

Finally, at the right end plate

$$U_N(r,\varphi,z_N=L_N) = 0 \quad \text{on } S_{\mathrm{III}} \tag{17}$$

Mode matching method

The calculation of the modal amplitudes $A^{\pm}$, $B^{\pm}$ for the ducts I, II, III, 1, 2, …, N requires the generation of a suitable algebraic system of equation. The mode matching technique [9] is then applied, considering first the continuity of pressure at the inlet, Eq. (8). This is multiplied by $\psi_{\mathrm{I},ts}(r_{\mathrm{I}})\,\mathrm{e}^{\mathrm{j}t\varphi_{\mathrm{I}}}$, t = 0, 1, 2, …, t_{max} and s = 0, 1, 2, …, s_{max}, and integrated over S_{I}, giving

$$\begin{aligned} &\int_{S_{\mathrm{I}}} P_{\mathrm{I}}(r_{\mathrm{I}},\varphi_{\mathrm{I}},z=0)\,\psi_{\mathrm{I},ts}(r_{\mathrm{I}})\,\mathrm{e}^{\mathrm{j}t\varphi_{\mathrm{I}}}\,\mathrm{d}S \\ &= \int_{S_{\mathrm{I}}} P_{\mathrm{III}}(r,\varphi,z=0)\,\psi_{\mathrm{I},ts}(r_{\mathrm{I}})\,\mathrm{e}^{\mathrm{j}t\varphi_{\mathrm{I}}}\,\mathrm{d}S \end{aligned} \tag{18}$$

The same procedure is applied again to Eq. (8), with $\psi_{\mathrm{I},ts}(r_{\mathrm{I}})\,\mathrm{e}^{-\mathrm{j}t\varphi_{\mathrm{I}}}$, t = 1, 2, …, t_{max} and s = 0, 1, 2, …, s_{max}, yielding

$$\begin{aligned} &\int_{S_{\mathrm{I}}} P_{\mathrm{I}}(r_{\mathrm{I}},\varphi_{\mathrm{I}},z=0)\,\psi_{\mathrm{I},ts}(r_{\mathrm{I}})\,\mathrm{e}^{-\mathrm{j}t\varphi_{\mathrm{I}}}\,\mathrm{d}S \\ &= \int_{S_{\mathrm{I}}} P_{\mathrm{III}}(r,\varphi,z=0)\,\psi_{\mathrm{I},ts}(r_{\mathrm{I}})\,\mathrm{e}^{-\mathrm{j}t\varphi_{\mathrm{I}}}\,\mathrm{d}S \end{aligned} \tag{19}$$

For the pressure at the outlet, Eq. (9) is multiplied by $\psi_{\mathrm{II},ts}(r_{\mathrm{II}})\mathrm{e}^{\mathrm{j}t\varphi_{\mathrm{II}}}$, t = 0, 1, 2, …, t_{max} and s = 0, 1, 2, …, s_{max}, and integrated over S_{II}, providing

$$\begin{aligned}&\int_{S_{\mathrm{II}}} P_{\mathrm{II}}(r_{\mathrm{II}},\varphi_{\mathrm{II}},z=0)\psi_{\mathrm{II},ts}(r_{\mathrm{II}})\mathrm{e}^{\mathrm{j}t\varphi_{\mathrm{II}}}\,\mathrm{d}S\\&=\int_{S_{\mathrm{II}}} P_{\mathrm{III}}(r,\varphi,z=0)\psi_{\mathrm{II},ts}(r_{\mathrm{II}})\mathrm{e}^{\mathrm{j}t\varphi_{\mathrm{II}}}\,\mathrm{d}S\end{aligned} \tag{20}$$

With $\psi_{\mathrm{II},ts}(r_{\mathrm{II}})\mathrm{e}^{-\mathrm{j}t\varphi_{\mathrm{II}}}$, t = 1, 2, …, t_{max} and s = 0, 1, 2, …, s_{max}, the expressions derived from Eq. (9) are

$$\begin{aligned}&\int_{S_{\mathrm{II}}} P_{\mathrm{II}}(r_{\mathrm{II}},\varphi_{\mathrm{II}},z=0)\psi_{\mathrm{II},ts}(r_{\mathrm{II}})\mathrm{e}^{-\mathrm{j}t\varphi_{\mathrm{II}}}\,\mathrm{d}S\\&=\int_{S_{\mathrm{II}}} P_{\mathrm{III}}(r,\varphi,z=0)\psi_{\mathrm{II},ts}(r_{\mathrm{II}})\mathrm{e}^{-\mathrm{j}t\varphi_{\mathrm{II}}}\,\mathrm{d}S\end{aligned} \tag{21}$$

Eqs. (10), (11) and (12), associated with the velocity conditions at the left side of the muffler, are multiplied by $\psi_{\mathrm{III},ts}(r)\mathrm{e}^{\mathrm{j}t\varphi}$, t = 0, 1, 2, …, t_{max} and s = 0, 1, 2, …, s_{max}, and integrated over S_{I}, S_{II} and $S_{\mathrm{III}} - S_{\mathrm{II}} - S_{\mathrm{I}}$, respectively. Then, the integrals are added, giving

$$\begin{aligned}&\int_{S_{\mathrm{I}}} U_{\mathrm{I}}(r_1,\varphi_1,z=0)\psi_{\mathrm{III},ts}(r)\mathrm{e}^{\mathrm{j}t\varphi}\,\mathrm{d}S\\&+\int_{S_{\mathrm{II}}} U_{\mathrm{II}}(r_{\mathrm{II}},\varphi_{\mathrm{II}},z=0)\psi_{\mathrm{III},ts}(r)\mathrm{e}^{\mathrm{j}t\varphi}\,\mathrm{d}S\\&=\int_{S_{\mathrm{III}}} U_{\mathrm{III}}(r,\varphi,z=0)\psi_{\mathrm{III},ts}(r)\mathrm{e}^{\mathrm{j}t\varphi}\,\mathrm{d}S\end{aligned} \tag{22}$$

The previous procedure, with $\psi_{\mathrm{III},ts}(r)\mathrm{e}^{-\mathrm{j}t\varphi}$, t = 1, 2, …, t_{max} and s = 0, 1, 2, …, s_{max}, is applied again to Eqs. (10), (11) and (12), which yields

$$\begin{aligned}&\int_{S_{\mathrm{I}}} U_{\mathrm{I}}(r_1,\varphi_1,z=0)\psi_{\mathrm{III},ts}(r)\mathrm{e}^{-\mathrm{j}t\varphi}\,\mathrm{d}S\\&+\int_{S_{\mathrm{II}}} U_{\mathrm{II}}(r_{\mathrm{II}},\varphi_{\mathrm{II}},z=0)\psi_{\mathrm{III},ts}(r)\mathrm{e}^{-\mathrm{j}t\varphi}\,\mathrm{d}S\\&=\int_{S_{\mathrm{III}}} U_{\mathrm{III}}(r,\varphi,z=0)\psi_{\mathrm{III},ts}(r)\mathrm{e}^{-\mathrm{j}t\varphi}\,\mathrm{d}S\end{aligned} \tag{23}$$

The integrals associated with Eqs. (18)-(23) can be evaluated analytically considering the properties of the Bessel functions in combination with Graf's addition theorem [9,10].

For the perforated plate, and in view of the orthogonality properties of the Bessel functions [10], the continuity of velocity expressed by Eq. (13) leads, for t = 0, 1, 2, …, t_{max} and s = 0, 1, 2, …, s_{max}, to

$$\begin{aligned}&\left(k_{\mathrm{III},ts}/\rho_0\right)\left(A^{+}_{\mathrm{III},ts}\,\mathrm{e}^{-\mathrm{j}k_{ts}L_0} - B^{+}_{\mathrm{III},ts}\,\mathrm{e}^{\mathrm{j}k_{ts}L_0}\right)\\&=\left(\tilde{k}_{1,ts}/\tilde{\rho}\right)\left(A^{+}_{1,ts} - B^{+}_{1,ts}\right)\end{aligned} \tag{24}$$

and for t = 1, 2, …, t_{max} and s = 0, 1, 2, …, s_{max},

$$\begin{aligned}&\left(k_{\mathrm{III},ts}/\rho_0\right)\left(A^{-}_{\mathrm{III},ts}\,\mathrm{e}^{-\mathrm{j}k_{ts}L_0} - B^{-}_{\mathrm{III},ts}\,\mathrm{e}^{\mathrm{j}k_{ts}L_0}\right)\\&=\left(\tilde{k}_{1,ts}/\tilde{\rho}\right)\left(A^{-}_{1,ts} - B^{-}_{1,ts}\right)\end{aligned} \tag{25}$$

The pressure-velocity relationship given by Eq. (14) yields, for t = 0, 1, 2, …, t_{max} and s = 0, 1, 2, …, s_{max},

$$\begin{aligned}&A^{+}_{\mathrm{III},ts}\,\mathrm{e}^{-\mathrm{j}k_{ts}L_0}\left(\tilde{Z}_p\,k_{\mathrm{III},ts}/(\rho_0\,\omega)-1\right)\\&-B^{+}_{\mathrm{III},ts}\,\mathrm{e}^{\mathrm{j}k_{ts}L_0}\left(\tilde{Z}_p k_{\mathrm{III},ts}/(\rho_0\,\omega)+1\right)=-\left(A^{+}_{1,ts}+B^{+}_{1,ts}\right)\end{aligned} \tag{26}$$

and for t = 1, 2, …, t_{max} and s = 0, 1, 2, …, s_{max},

$$\begin{aligned}&A^{-}_{\mathrm{III},ts}\,\mathrm{e}^{-\mathrm{j}k_{ts}L_0}\left(\tilde{Z}_p\,k_{\mathrm{III},ts}/(\rho_0\,\omega)-1\right)\\&-B^{-}_{\mathrm{III},ts}\,\mathrm{e}^{\mathrm{j}k_{ts}L_0}\left(\tilde{Z}_p k_{\mathrm{III},ts}/(\rho_0\,\omega)+1\right)=-\left(A^{-}_{1,ts}+B^{-}_{1,ts}\right)\end{aligned} \tag{27}$$

At the interface between dissipative regions i and i + 1, for i = 1, 2, …, N – 1, the continuity of pressure expressed by Eq. (15) yields, for t = 0, 1, 2, …, t_{max} and s = 0, 1, 2, …, s_{max},

$$A^{+}_{i,ts}\,\mathrm{e}^{-\mathrm{j}\tilde{k}_{i,ts}L_i} + B^{+}_{i,ts}\,\mathrm{e}^{\mathrm{j}k_{i,ts}L_i} = A^{+}_{i+1,ts} + B^{+}_{i+1,ts} \tag{28}$$

and for t = 1, 2, …, t_{max} and s = 0, 1, 2, …, s_{max},

$$A^{-}_{i,ts}\,\mathrm{e}^{-\mathrm{j}\tilde{k}_{i,ts}L_i} + B^{-}_{i,ts}\,\mathrm{e}^{\mathrm{j}k_{i,ts}L_i} = A^{-}_{i+1,ts} + B^{-}_{i+1,ts} \tag{29}$$

Considering again the interface between dissipative regions i and i + 1, for i = 1, 2, …, N – 1, the continuity of velocity given by Eq. (16) yields, for t = 0, 1, 2, …, t_{max} and s = 0, 1, 2, …, s_{max},

$$\begin{aligned}&\left(\tilde{k}_{i,ts}/\tilde{\rho}_i\right)\left(A^{+}_{i,ts}\,\mathrm{e}^{-\mathrm{j}k_{i,ts}L_i} - B^{+}_{i,ts}\,\mathrm{e}^{\mathrm{j}k_{i,ts}L_i}\right)\\&=\left(\tilde{k}_{i+1,ts}/\tilde{\rho}_{i+1}\right)\left(A^{+}_{i+1,ts} - B^{+}_{i+1,ts}\right)\end{aligned} \tag{30}$$

and for t = 1, 2, …, t_{max} and s = 0, 1, 2, …, s_{max},

$$\begin{aligned}&\left(\tilde{k}_{i,ts}/\tilde{\rho}_i\right)\left(A^{-}_{i,ts}\,\mathrm{e}^{-\mathrm{j}k_{i,ts}L_i} - B^{-}_{i,ts}\,\mathrm{e}^{\mathrm{j}k_{i,ts}L_i}\right)\\&=\left(\tilde{k}_{i+1,ts}/\tilde{\rho}_{i+1}\right)\left(A^{-}_{i+1,ts} - B^{-}_{i+1,ts}\right)\end{aligned} \tag{31}$$

Finally, the right end plate condition defined by Eq. (17) provides, for t = 0, 1, 2, …, t_{max} and s = 0, 1, 2, …, s_{max},

$$B^{+}_{N,ts} = A^{+}_{N,ts}\,\mathrm{e}^{-\mathrm{j}2k_{ts}L_N} \tag{32}$$

and for t = 1, 2, …, t_{max} and s = 0, 1, 2, …, s_{max},

$$B^{-}_{N,ts} = A^{-}_{N,ts}\,\mathrm{e}^{-\mathrm{j}2k_{ts}L_N} \tag{33}$$

The system associated with Eqs. (18)-(33) is calculated with the truncation $m_{max} = t_{max}$ and $n_{max} = s_{max}$. Also, an incident plane wave is considered as acoustic excitation, $A^{+}_{1,00}=1$, while an anechoic termination is imposed at the outlet, $P_{\mathrm{AII}} = 0$ ($A^{\pm}_{\mathrm{II},mn}=0$ for all m and n). A final system of 2 (N + 2) (2 t_{max} + 1) (s_{max} + 1) equations is then solved, providing the modal amplitudes in all the ducts shown in Figure 1, $B^{\pm}_{\mathrm{I}}, B^{\pm}_{\mathrm{II}}, A^{\pm}_{\mathrm{III}}, B^{\pm}_{\mathrm{III}}, A^{\pm}_{1}, B^{\pm}_{1}, A^{\pm}_{2}, B^{\pm}_{2}, \ldots, A^{\pm}_{N}, B^{\pm}_{N}$. The attenuation, calculated via the transmission loss, is given by

$$TL = -20\log\left(\frac{R_{\mathrm{II}}}{R_{\mathrm{I}}}\left|B^{+}_{\mathrm{II},00}\right|\right) \tag{34}$$

RESULTS AND DISCUSSION

Reactive mufflers

First, a circular reactive reversing chamber muffler is considered for illustration purposes, with the absence of absorbent material and perforated plate. The relevant geometrical dimensions are detailed in Table 1. The calculations are carried out with $t_{max} = s_{max} = 5$ modes, which guarantee an accurate prediction of the acoustic behaviour [9].

To obtain a good attenuation performance, the inlet is centred and the outlet is offset and located on the nodal line of the mode (0,1), at a distance δ_{II} = 0.6276 R_{II} = 0.05648 m from the centre [9]. This "optimum" offset extends the acoustic performance beyond the asymmetric higher order modes (1,0) and (2,0) (with associated frequencies 1107 Hz and 1836 Hz, respectively, for 15ºC) and also the axisymmetric mode (0,1), with 2304 Hz.

Table 1. Geometry of reactive muffler

Geom.	R_I, R_{II} (m)	R_{III}(m)	L_0 (m)	δ_I (m)	δ_{II} (m)
1	0.02	0.09	0.25	0.0	0.056

Figure 2 shows the transmission loss curves depicted as a function of frequency. The expected shift towards high frequencies is found as the temperature increases.

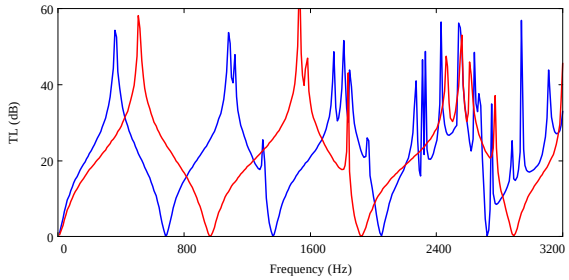

Figure 2. *TL* of circular reactive reversing chamber muffler, geometry 1: ———, T = 15 ºC; ———, T = 300 ºC.

Figure 3 shows the same attenuations, now plotted as a function of the normalized frequency $f/c_0(T)$. Both curves appear overlapped, as expected. Thus, with a single calculation at a known temperature, the acoustic attenuation performance can be evaluated for a wide temperature range.

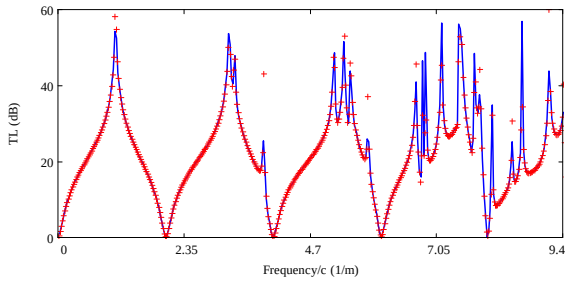

Figure 3. *TL* of circular reactive reversing chamber muffler, geometry 1, considering $f/c_0(T)$ as the abscissa: ———, T = 15 ºC; + + + +, T = 300 ºC.

Influence of temperature in dissipative configurations

A circular dissipative reversing chamber muffler [7] is now considered (see Figure 1 for details), with N = 1 and uniform temperature in all the regions involved (I, II, III and 1). For the absorbent material (Owens Corning's texturized fibre glass roving), a modified version of the model presented by Delany and Bazley [11] is used, where the characteristic impedance $\tilde{Z} = \tilde{\rho}\,\tilde{c}$ and the wavenumber $\tilde{k} = \omega/\tilde{c}$ are expressed as [12]

$$\tilde{Z} = Z_0\left(\left(1 + a_5\left(\frac{f\,\rho_0}{R}\right)^{-a_6}\right) + \mathrm{j}\left(-a_7\left(\frac{f\,\rho_0}{R}\right)^{-a_8}\right)\right) \tag{35}$$

$$\tilde{k} = k_0\left(\left(1 + a_3\left(\frac{f\,\rho_0}{R}\right)^{-a_4}\right) + \mathrm{j}\left(-a_1\left(\frac{f\,\rho_0}{R}\right)^{-a_2}\right)\right) \tag{36}$$

$Z_0 = \rho_0\, c_0$ being the characteristic impedance of the air and R the steady airflow resistivity, with the values R = 4896 rayl/m and R = 1000 rayl/m at room temperature for packing densities of 100 kg/m^3 and 42 kg/m^3, respectively [7,13]. The coefficients a_i, i = 1, 2, …, 8, are given in Table 2.

Table 2. Coefficients for Owens Corning's fibre

a_1	a_2	a_3	a_4	a_5	a_6	a_7	a_8
0.18897	0.595	0.16	0.577	0.09534	0.754	0.08504	0.732

The acoustic impedance of the perforated plate is calculated by [12]

$$\tilde{Z}_p = Z_0\,\frac{\left(0.006 + \mathrm{j}k_0\left(t_p + 0.425\,d_h\left(1 + \frac{\tilde{Z}}{Z_0}\frac{\tilde{k}}{k_0}\right)F(\sigma)\right)\right)}{\sigma} \tag{37}$$

where d_h denotes the hole diameter, t_p the thickness, σ the porosity and $F(\sigma)$ accounts for the interaction between perforations. Here the following expression is considered [12]

$$F(\sigma) = 1 - 1.055\sqrt{\sigma} + 0.17\left(\sqrt{\sigma}\right)^3 + 0.035\left(\sqrt{\sigma}\right)^5 \tag{38}$$

Table 3 provides the details of the dissipative configuration under consideration. The geometry is basically similar to the reversing chamber of Table 1, now including a region with absorbent material of length L_1 = 0.25 m and a perforated plate characterised by the values d_h = 0.0035 m, t_p = 0.001 m and σ = 0.25.

Table 3. Geometry of dissipative muffler

Geom.	R_I, R_{II} (m)	R_{III}(m)	L_0 (m)	L_1 (m)	δ_I (m)	δ_{II} (m)
2	0.02	0.09	0.25	0.25	0.0	0.056

Figure 4 shows the transmission loss curves depicted as a function of frequency. Calculations have been carried out for 15 ºC and 300 ºC (uniform temperature in all the regions involved I, II, III and 1). In the latter case (300 ºC), two situations are analysed. On one hand, Eqs. (35)-(37) include the effect of temperature via the values of Z_0, ρ_0 and k_0 evaluated at T = 300 ºC, but neither a_i nor R are modified (and the value R = 1000 is used). On the other hand, the influence of temperature is taken into account for Z_0, ρ_0 and k_0 and it is also extended to the resistivity R by the expression [14]

$$R(T) = R(T_0)\,\frac{\mu(T)}{\mu(T_0)} \tag{39}$$

where μ is the dynamic viscosity of the air and the temperatures T, T_0 are in Kelvin. The approximate value R = 1636 rayl/m is obtained for T = 300 ºC if the value R = 1000 rayl/m is associated with T = 15 ºC. As can be seen in the figure, both calculations at T = 300 ºC exhibit the expected shift towards high frequencies in comparison with the transmission loss at room temperature (blue line). Comparing the attenuations at T = 300 ºC (red and black lines), this associated with the adapted resistivity (black line) provides higher relative minima and lower relative maxima, as expected [7].

Figure 4 also includes a validation of the analytical results (for the configuration with T = 300 ºC and R = 1636 rayl/m), obtained by a numerical calculation based on the finite element method (FEM), considering 10-noded tetrahedral elements with an approximate element size of 0.01 m. Analytical and FEM results are essentially identical, with overlapped curves throughout the entire frequency range of interest, thus providing a validation for the analytical procedure.

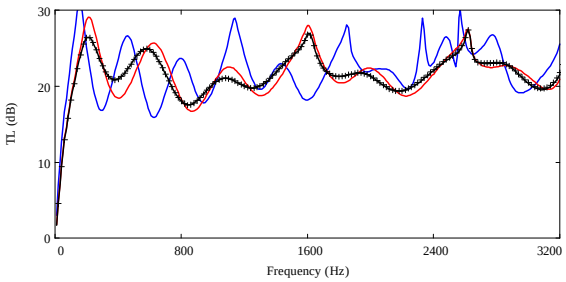

Figure 4. *TL* of circular dissipative reversing chamber muffler, geometry 2: ———, T = 15 ºC, R = 1000 rayl/m; ———, T = 300 ºC, R = 1000 rayl/m; ———, T = 300 ºC, R = 1636 rayl/m; + + + +, T = 300 ºC, R = 1636 rayl/m, FEM.

Figure 5 depicts the transmission loss shown in Figure 4, now plotted as a function of the normalized frequency $f/c_0(T)$. The behaviour observed in Figure 3 for a reactive configuration is not present for the dissipative configurations, since the overlapping does not longer hold, mainly in the low and mid frequency range. Therefore, a specific calculation is required for each temperature, at least under the hypotheses established in the current investigation and with the models of impedance and wavenumber currently available in the literature for the absorbent material. More experimentation is required to provide further information related to possible variations of coefficients a_i as the temperature increases.

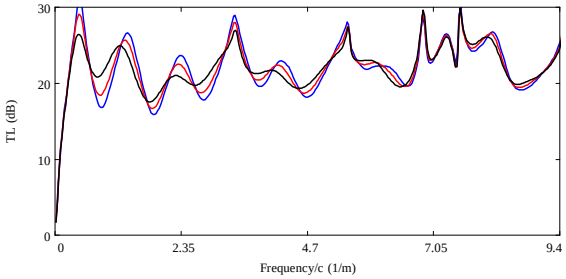

Figure 5. *TL* of circular dissipative reversing chamber muffler, geometry 2, considering $f/c_0(T)$ as the abscissa: ———, T = 15 ºC, R = 1000 rayl/m; ———, T = 300 ºC, R = 1000 rayl/m; ———, T = 300 ºC, R = 1636 rayl/m.

Temperature gradients

Tables 4 and 5 show the details for the consideration of temperature gradients within the absorbent material. The left side of the absorbent material is at temperature T_1 = 300 ºC, while the value associated with the right side is T_{N+1} = 100 ºC. This temperature gradient, higher than the values found in automotive applications, is used for illustration purposes. For geometries 3 and 4, the number of segments with uniform temperature is N = 2 and N = 3, respectively. For comparison, geometry 2 (see Tables 3 and 5) is also included in the results shown in Figure 6 for two cases: (1) with uniform temperature (300 ºC) in the absorbent material and (2) with a single segment at temperature $\tilde{T}_1$ = 200 ºC.

In all the cases, uniform temperature is assumed for regions I, II and III (air), with an associated value T = 300 ºC. In each segment i, the absorbent material is characterised by Eqs. (35) and (36), with the values Z_0, ρ_0, k_0 and R at temperature $\tilde{T}_i$, the resistivity being calculated via Eq. (39). The perforated plate is not included in this section, that is, $\tilde{Z}_p = 0$.

Table 4. Geometry of dissipative mufflers

Geom.	R_I, R_{II} (m)	R_{III}(m)	L_0 (m)	L_1 (m)	L_2 (m)	L_3 (m)
3	0.02	0.09	0.25	0.25/2	0.25/2	0.0
4	0.02	0.09	0.25	0.25/3	0.25/3	0.25/3

Table 5. Temperatures associated with the regions (ºC)

Geom.	T_1	T_2	T_3	T_4	$\tilde{T}_1$	$\tilde{T}_2$	$\tilde{T}_3$
2	300	100	--	--	200	--	--
3	300	200	100	--	250	150	--
4	300	233.3	166.7	100	266.7	200	133.3

As can be observed in Figure 6, the presence of a temperature gradient slightly modifies the acoustic performance in comparison with the case of uniform temperature. The effect of this gradient, however, is accurately predicted with a single segment, N = 1, since the use of N = 2 and N = 3 produces nearly overlapped curves, with only very slight variations in the attenuation. Therefore, if the temperature field is not uniform within the dissipative region, the use of an average temperature is accurate enough for calculating the acoustic attenuation performance, at least for the values and spatial distribution assumed in the current work.

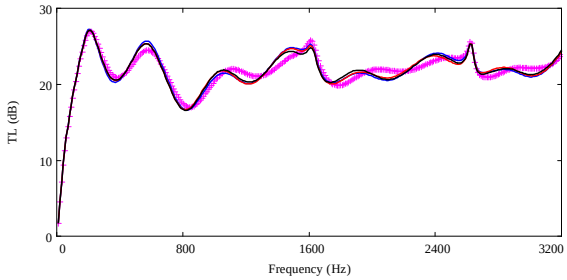

Figure 6. *TL* of circular dissipative reversing chamber muffler, $T_I = T_{II} = T_{III}$ = 300 ºC: + + + +, geometry 2, uniform temperature; ———, geometry 2, N = 1, $\tilde{T}_1$ = 200 ºC; ———, geometry 3, N = 2, $\tilde{T}_1$ = 250 ºC, $\tilde{T}_2$ = 150 ºC; ———, geometry 4, N = 3, $\tilde{T}_1$ = 266.7 ºC, $\tilde{T}_2$ = 200 ºC, $\tilde{T}_3$ = 133.3 ºC .

CONCLUSIONS

A multidimensional analytical approach based on the mode matching method has been presented for the acoustic analysis of circular dissipative reversing chamber mufflers with temperature gradients. To account for the variation of temperature within the absorbent material, a segmentation procedure has been considered with a number of dissipative regions with different but axially uniform temperature. The results provided by the analytical technique have been compared with numerical calculations based on the finite element method, showing a good agreement.

For reactive mufflers, the acoustic attenuation is not influenced by the temperature if a representation as a function of the normalized frequency $f/c_0(T)$ is carried out, with all the transmission loss curves being overlapped, as expected. Therefore, a single calculation at a known temperature allows the calculation of the acoustic attenuation performance for a wide temperature range.

The previous comments cannot be applied, in general, to dissipative mufflers, at least with the models of impedance and wavenumber currently available in the literature for absorbent materials. In this case, and with the hypotheses established in the current investigation, a specific calculation is required for each temperature. Further experimentation is needed to provide additional information related to the influence of temperature in the properties of absorbent materials used in the exhaust system of internal combustion engines.

Concerning the influence of temperature gradients, these have been shown to slightly modify the attenuation in comparison with the case of uniform temperature field for the configuration under analysis (circular dissipative reversing chamber mufflers) and for the gradient values assumed within the absorbent material. To provide an accurate prediction of the gradient influence, a single segment with the average temperature between both sides of the absorbent material has been found to be enough, even for the high value assumed for the temperature gradient.

ACKNOWLEDGEMENTS

The authors gratefully acknowledge the financial support of Ministerio de Ciencia e Innovación by means of the project DPI2007-62635.

REFERENCES

1 A. Selamet, M.B. Xu, I.J. Lee and N.T. Huff, "Dissipative expansion chambers with two concentric layers of fibrous materials" *Int. J. Vehicle Noise Vib.* **1**, 341-357 (2005)
2 A. Selamet, M.B. Xu, I.J. Lee and N.T. Huff, "Effects of voids on the acoustics of perforated dissipative silencers" *Int. J. Vehicle Noise Vib.* **2**, 357-372 (2006)
3 K.S. Peat and K.L. Rathi, "A finite element analysis of the convected acoustic wave motion in dissipative silencers" *J. Sound Vib.* **184**, 529-545 (1995)
4 K.S. Peat, "Convected acoustic wave motion along a capillary duct with an axial temperature gradient" *J. Sound Vib.* **203**, 855-866 (1997)
5 Y.H. Kim, J.W. Choi and B.D. Lim, "Acoustic characteristics of an expansion chamber with constant mass flow and steady temperature gradient (theory and numerical simulation)" *J. Vib. Acoust.* **112**, 460-467 (1990)
6 Y.H. Kim, J.W. Choi, "General solution of acoustic wave equation for circular reversing chamber with temperature gradient" *J. Vib. Acoust.* **113**, 543-550 (1991)
7 F.D. Denia, A. Antebas, A. Selamet, A.M. Pedrosa, "Acoustic characteristics of circular dissipative reversing chamber mufflers" *Submitted to Noise Control Eng. J.* (2010)
8 M.L. Munjal, *Acoustics of Ducts and Mufflers* (Wiley, New York, 1987)
9 A. Selamet and Z. L. Ji, "Acoustic attenuation performance of circular flow-reversing chambers" *J. Acoust. Soc. Am.* **104**, 2867-2877 (1998)
10 M. Abramowitz and I.A. Stegun, *Handbook of Mathematical Functions* (Dover Publications, New York, 1972)
11 M.E. Delany and E.N. Bazley, "Acoustical properties of fibrous absorbent materials" *Applied Acoust.* **3**, 105–116 (1970).
12 F.D. Denia, A. Selamet, F.J. Fuenmayor and R. Kirby, "Acoustic attenuation performance of perforated dissipative mufflers with empty inlet/outlet extensions" *J. Sound Vib.* **302**, 1000-1017 (2007)
13 A. Selamet, I.J. Lee and N.T. Huff, "Acoustic attenuation of hybrid silencers" *J. Sound Vib.* **262**, 509-527 (2003)
14 F.P. Mechel, *Formulas of Acoustics* (Springer, Berlin, 2004)